Supporting Information

Strategic B-Site Cation Engineering in Sillén-Aurivillius Perovskite Oxyhalides for Ultra-High Efficiency Piezocatalytic H_2O_2 Production

Yunxiang Zhang[a,b], Shishi Xu[a,b], Jikun Chen[a], Jiali Zhang[a], Zhichao Mu[a], Chenliang Zhou[a], Hazem Abdelsalam[a,c], Qinfang Zhang[a,b,]*

[a] School of Materials Science and Engineering, Yancheng Institute of Technology, Yancheng, 224051, PR China.

[b] Key Laboratory for Ecological-Environment Materials of Jiangsu Province, Yancheng Institute of Technology, Yancheng, 224051, PR China.

c Theoretical Physics Department, National Research Centre, El-Buhouth Str., 12622, Dokki, Giza, Egypt.

Corresponding author.

E-mail address: qfangzhang@gmail.com (Q. Zhang).

1. Characterization, DFT calculation, photoelectrochemical measurements, and photocatalytic degradation evaluation captions

1.1 Characterization

The surface topographies of all samples in this experiment were determined by scanning electron microscopy (SEM). A Philips X-ray diffraction (XRD) with Cu K_α radiation as the radiation source was conducted to determine the crystal structure of the prepared samples. The X-ray photoelectron spectroscopy (XPS) with Al Kα was employed to collect the information of chemical elements on Ag/$Bi_7Fe_2Ti_2O_{17}Cl$ material (Ag, Bi, Fe, Ti, Nb, O, Cl and C elements). Transmission electron microscopy (TEM) with energy dispersive spectrometer (EDS) patterns were obtained by using a JEOL JEM-2100F microscope. The UV-Vis diffuse reflectance spectra (DRS) was used to character the reflection (*R*) data of different $Bi_7Fe_2Ti_2O_{17}Cl$ samples. A Hitachi F-4600 fluorescence spectrophotometer was applied to measuring the photoluminescence (PL) spectra with the excitation lamp of a 150W Xe lamp at 400 V. Electrochemical impedance

spectroscopy (EIS) and transient photocurrent were measured by an electrochemical workstation of CHI-660D from Chenhua Instruments Co., Ltd.

1.2 Materials

The chemical reagents of bismuth nitrate ($Bi(NO_3)_3 \cdot 5H_2O$), potassium chloride (KCl), bismuth oxide (Bi_2O_3), and titanium dioxide (TiO_2) in this work are of analytical grade and used without further purification. And they are all bought from Shanghai Aladdin Reagent LTD.

1.3 Electrochemical and photoelectrochemical measurements

In this experiment, an electrochemical workstation was used to determine the electrochemical and photoelectrochemical measurements, which was equipped with a systematic three-electrode cell, including the working electrode of the as-prepared samples (1 × 1 cm^2), the reference electrode of Ag/AgCl (3 M KCl), and the counter electrode of Pt net (1.5 × 1.5 cm^2). The $BaBi_4TiNbO_{11}Cl$ powder of 5 mg was mixed with 0.5 % nafion of 1mL, and then the mixed solution was sonicated for 1 h at room temperature. Afterwards, the obtained solution was coated on a fluorine-doped tin oxide (FTO) substrate by using a squeezing method and dried at 60 °C for 4 h. The working electrode was prepared as follows: To measure the flat-band potential of instrument, impedance measurements were evaluated with the same electrodes in $NaSO_4$ electrolytic solution of 0.5 M (pH = 2).

2. Figure Captions

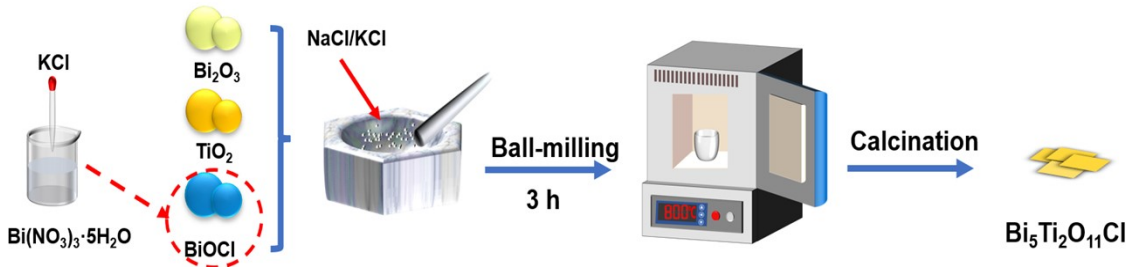

Fig. S1. Schematic illustration of the synthesis process of $Bi_5Ti_2O_{11}Cl$ nanoplates.

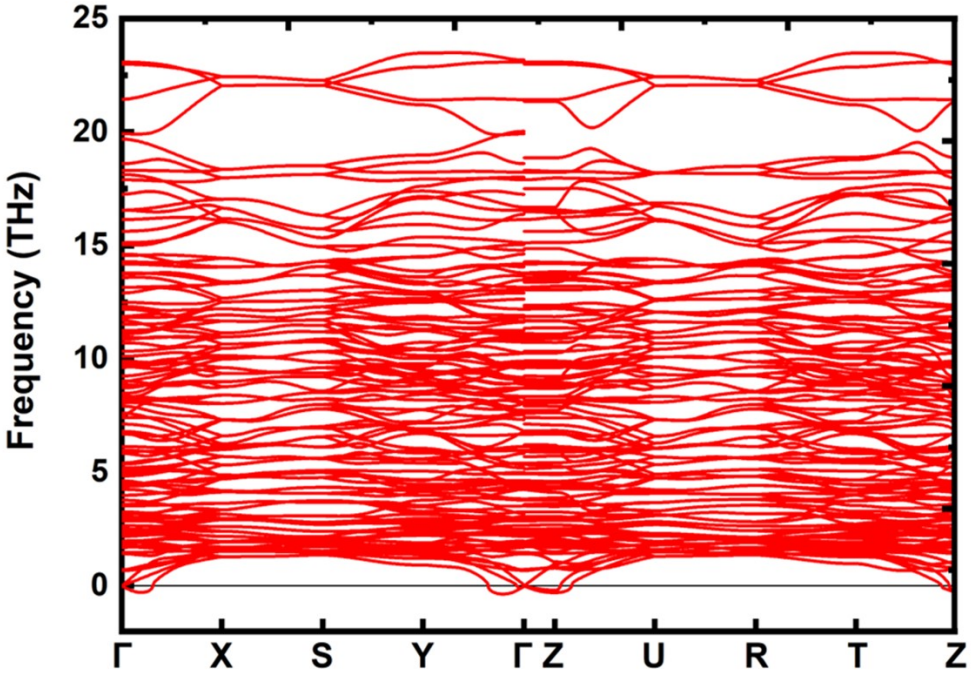

Fig. S2. Phonon-dispersion curves of $Bi_5Ti_2O_{11}F$.

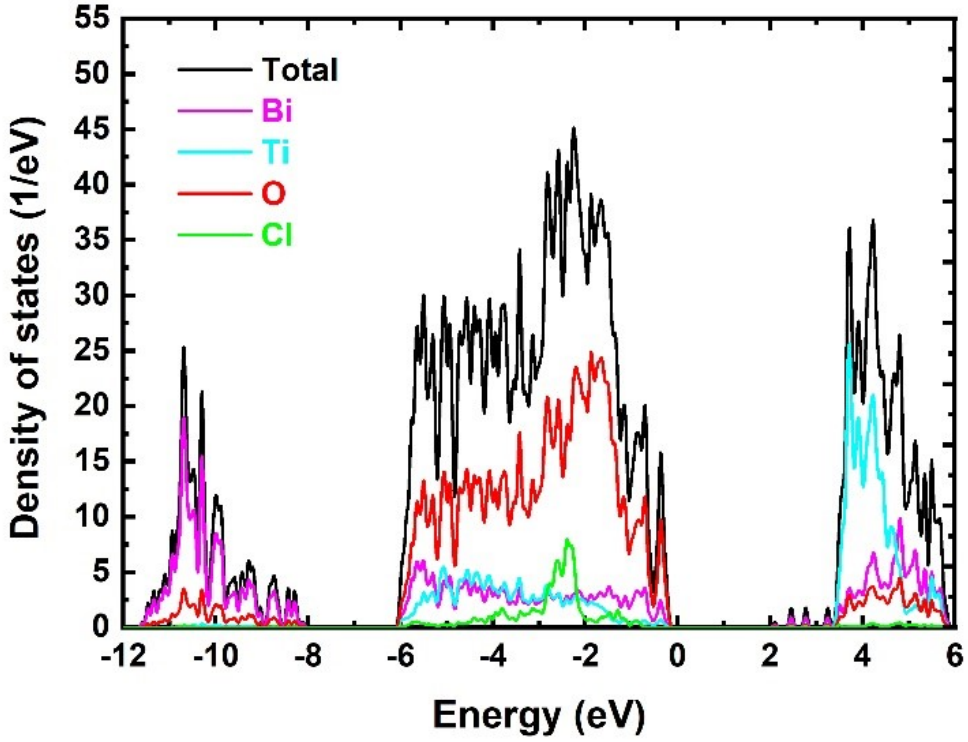

Fig. S3. Total density of states of $Bi_5Ti_2O_{11}Cl$.

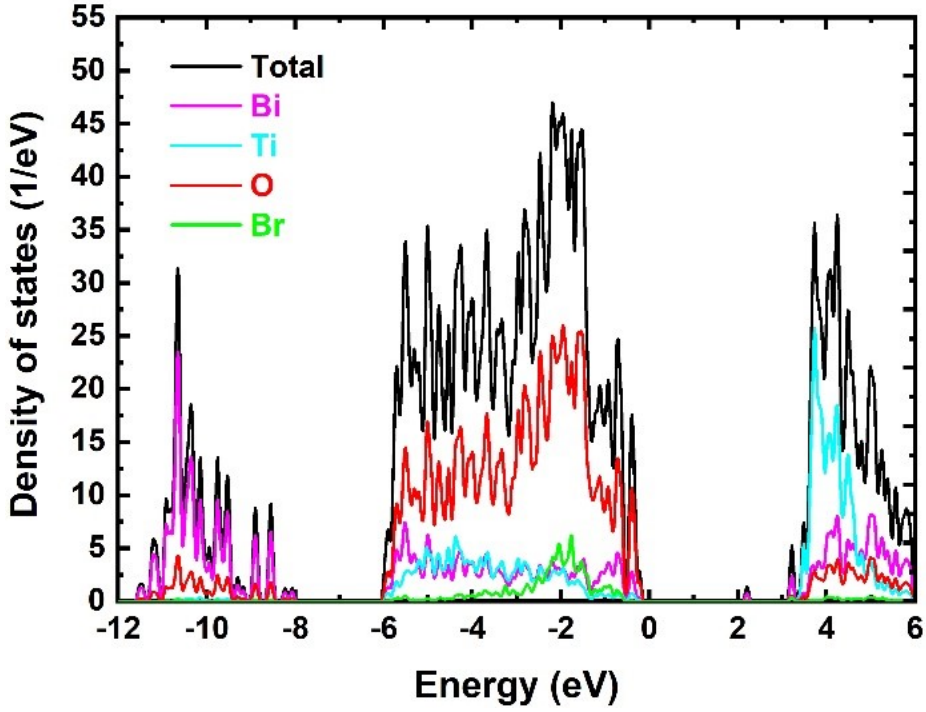

Fig. S4. Total density of states of $Bi_5Ti_2O_{11}Br$.

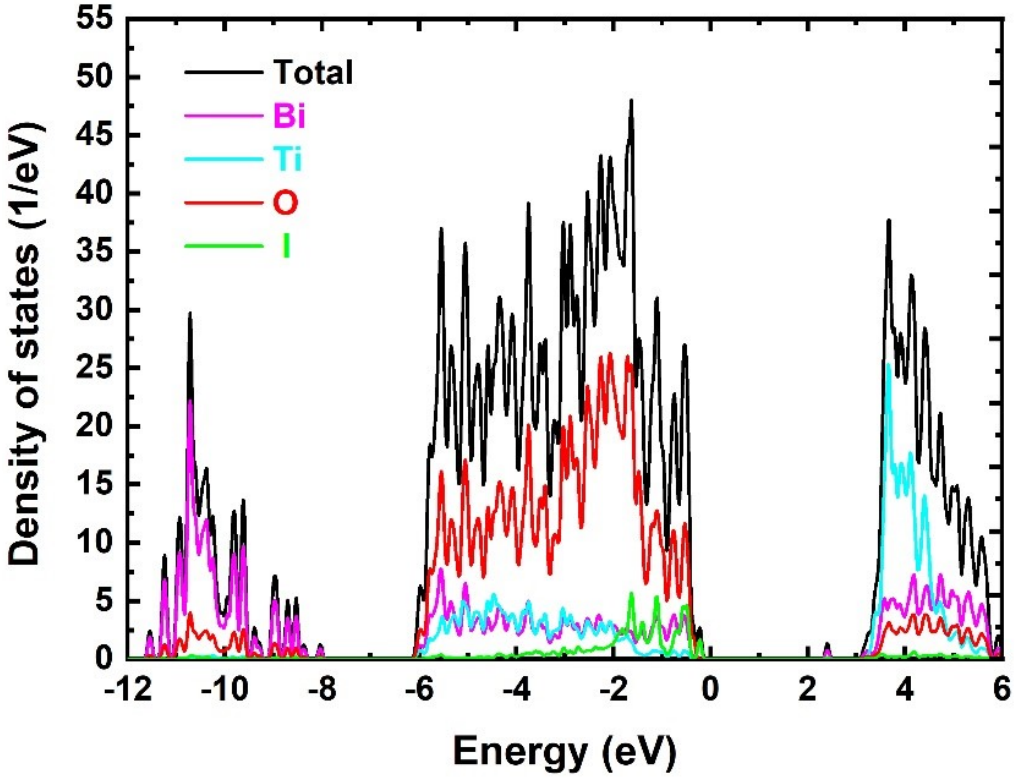

Fig. S5. Total density of states of $Bi_5Ti_2O_{11}I$.

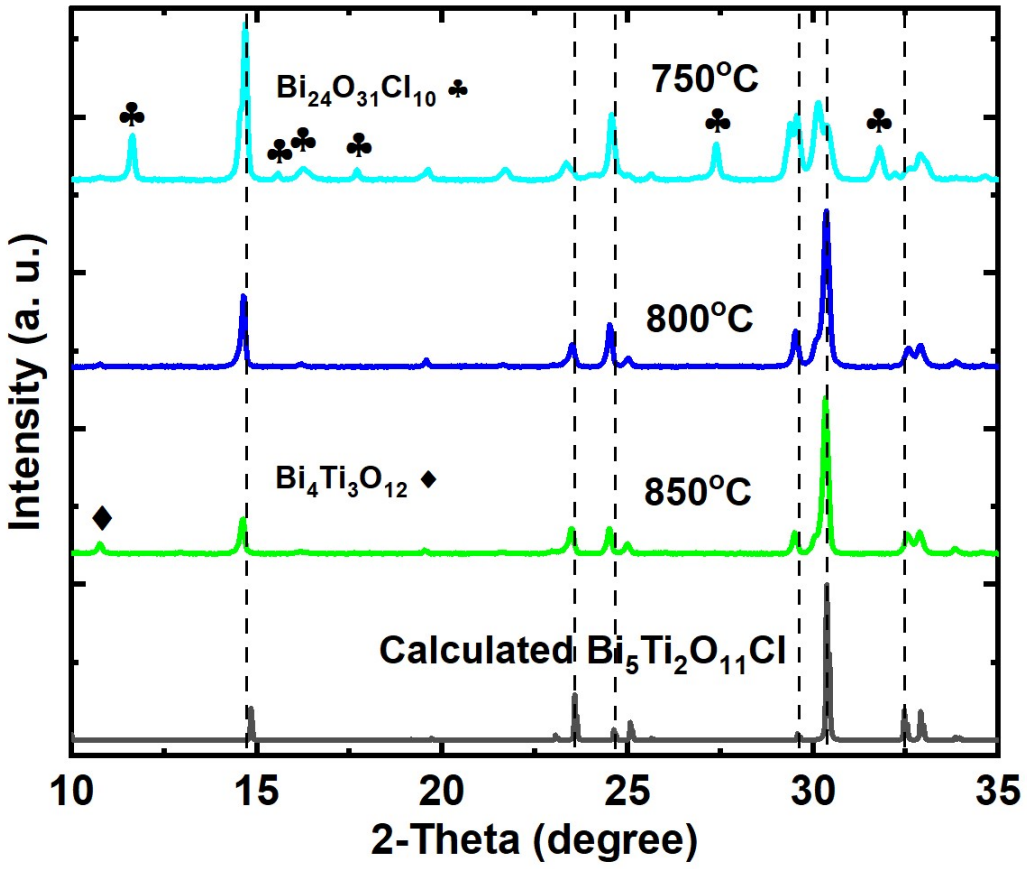

Fig. S6. The enlarged XRD patterns of samples in the range of 10 - 35 ° in Figure 2(a).

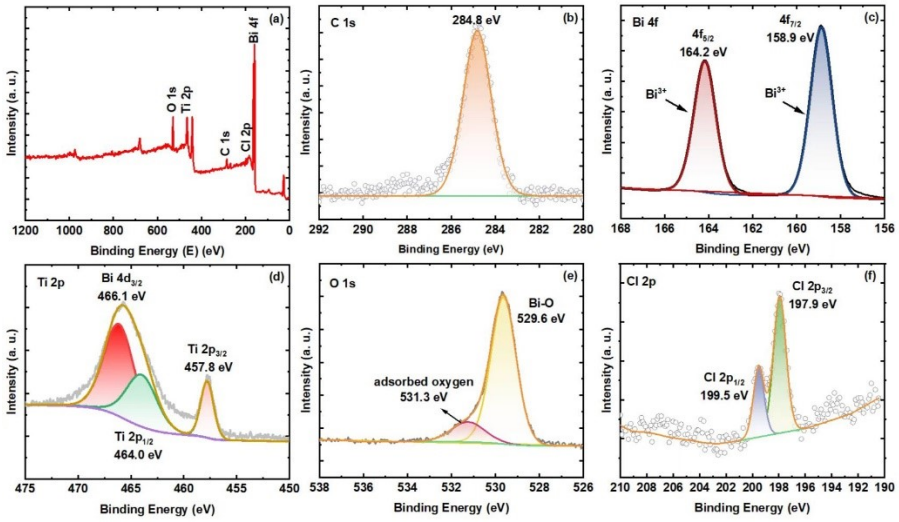

Fig. S7. XPS spectra of Bi-4*f* (a), Ti-2*p* (b), O-1*s* (c), and Cl-2*p* (d) for $Bi_5Ti_2O_{11}Cl$ nanoplates.

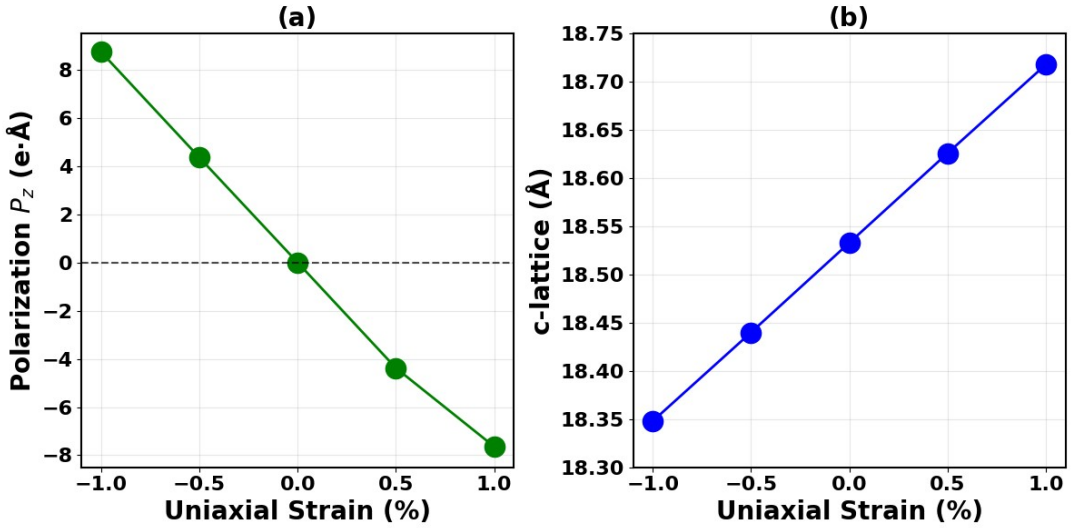

Fig. S8. Strain-dependent properties of $Bi_5Ti_2O_{11}Cl$ showing (a) out-of-plane polarization pz and (b) c-lattice parameter.

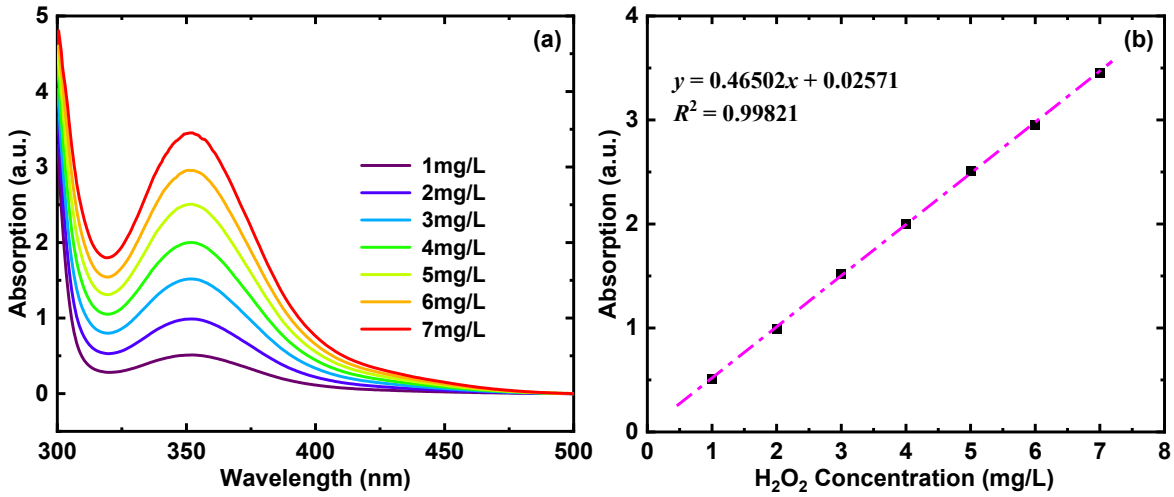

Fig. S9. the standard H_2O_2 concentration curves

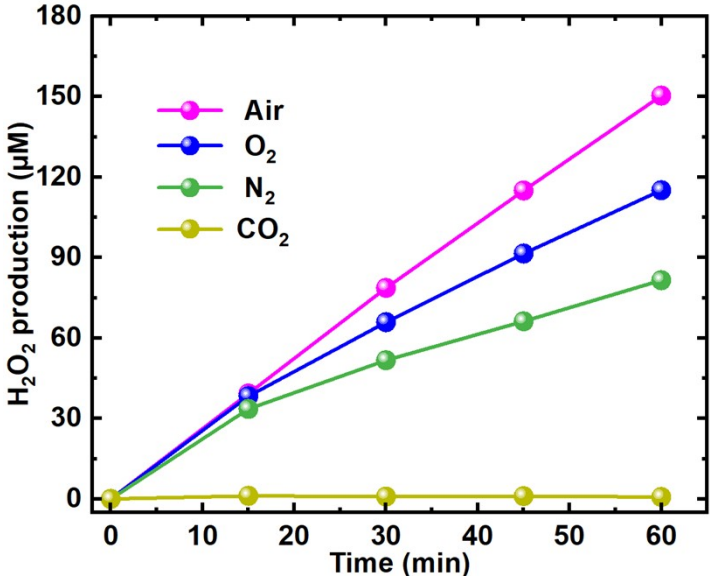

Fig. S10. The time-dependent curves of H_2O_2 production for piezocatalytic process with different atmospheres.

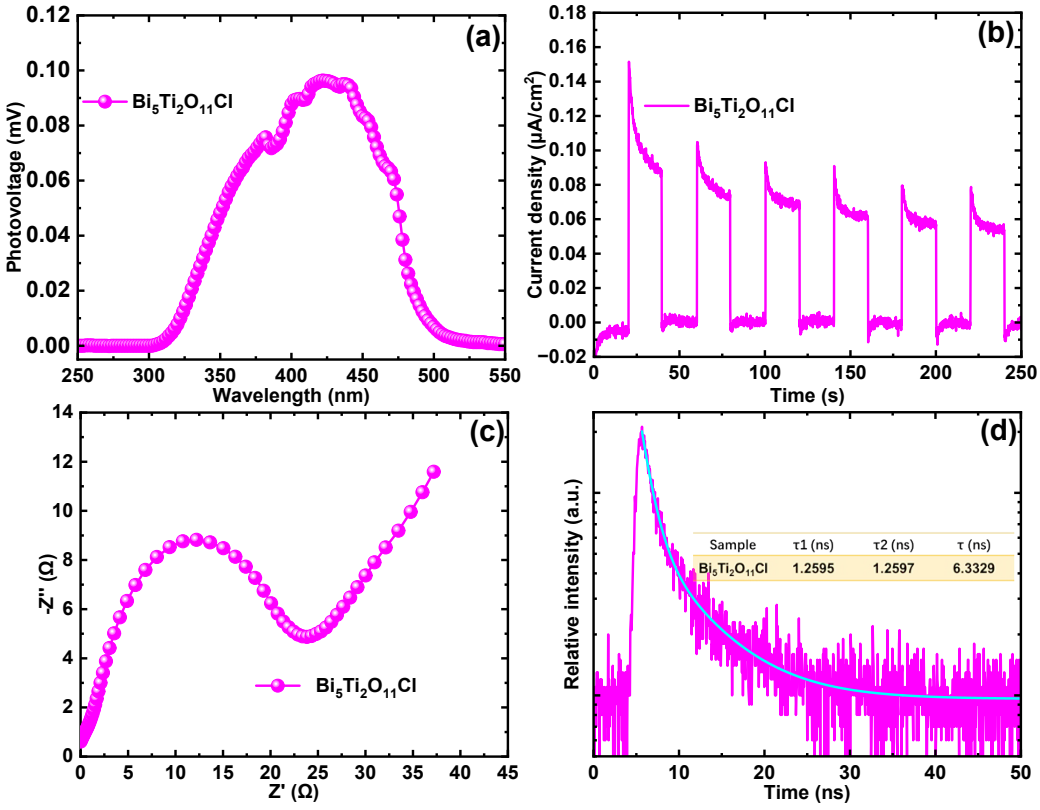

Fig. S11. (a) surface photovoltage (SPV) spectra, (b) Transient photocurrent response curves, (c) electrochemical impedance spectroscopy (EIS), and (d) the time-resolved PL (TR-PL) signals of as-synthesized photocatalyst

The separation and migration activities of photogenerated carriers were assessed on the raw $Bi_5Ti_2O_{11}Cl$ by the surface photovoltage (SPV) method, transient photocurrent response, electrochemical impedance spectroscopy (EIS), and time-resolved photoluminescence (TRPL), as depicted in **Fig. S11**. The dynamical charge transport of Sillén-Aurivillius oxyhalides induced by the created electric field were evaluated using SPV method, and this result was provided in **Fig. S11a**. The intensity of SPV for $Bi_5Ti_2O_{11}Cl$ is higher than that of Sillén-Aurivillius material of $Bi_7Fe_2Ti_2O_{17}Cl$, which was reported in our previous works (J. Mater. Chem. A, 2025, 13, 7989). This result may be ascribed to the enhanced IEF by high crystalline quality and stable crystal structure. Simultaneously, similar results also occur in PL, EIS and TRPL (Materials Today Energy 40 (2024) 101498; International Journal of Hydrogen Energy 59 (2024) 1156–1165), indicating that $Bi_5Ti_2O_{11}Cl$ has excellent charge separation and transfer efficiency.

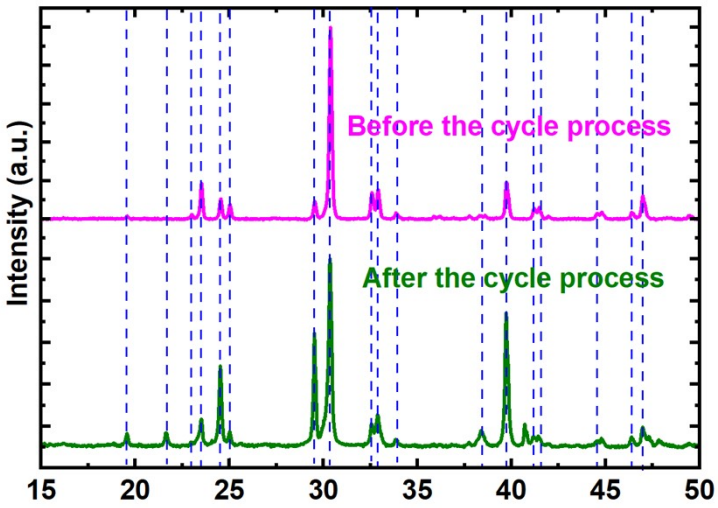

Fig. S12. The XRD patterns of the raw and used samples after fourth cycles.

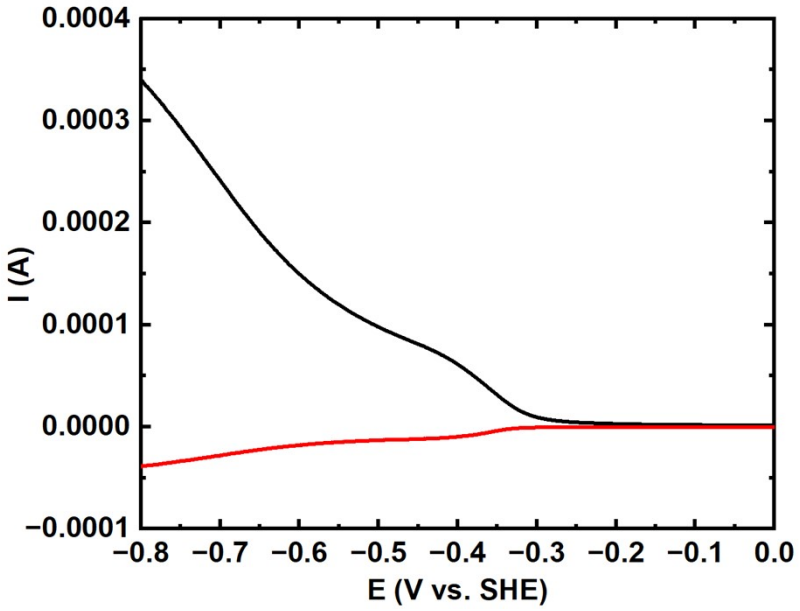

Fig. S13 LSV curves of $Bi_5Ti_2O_{11}Cl$ with RRDE

Table S1. Strain-dependent structural and electronic properties of $Bi_5Ti_2O_{11}Cl$ under uniaxial strain along the polar c-axis. Listed are the out-of-plane lattice parameter (c), and the electronic contribution to the out-of-plane polarization (pz).

Strain (%)	c (Å)	p_z (e·Å)
–1	18.348	8.74
–0.5	18.440	4.36
0	18.533	-0.001
+0.5	18.626	-4.38
+1	18.718	-7.64

Table S2. Statistics on the production rate of hydrogen peroxide in recent years.

No.	Samples	Generation rate(umol/g/h)	Solvent	References
1	COF-DH-Eth	9212	H_2O	https://doi.org/10.1002/anie.anie.202420218
2	TiO_{2-X}/g-C_3N_4	1780.3	H_2O	https://doi.org/10.1016/j.jmst.2024.02.048
3	g-C_3N_4/PCN-224	4860	H_2O	https://www.cjcatal.com/CN/10.1016/S1872-2067(23)64629-7
4	$ZnIn_2S_4$–$CdIn_2S_4$	843.02	H_2O	https://doi.org/10.1021/acscatal.4c00924
5	C_3N_{5-x}-CN	1359	H_2O	https://doi.org/10.1016/j.apcatb.2023.122752

6	PC-MB	1385.42	H_2O	https://doi.org/10.1039/D0TA03974H
7	SnS_2/In_2S_3/CDs	1111.89	H_2O	https://doi.org/10.1039/ D0TA10231H
8	$KSr_2Nb_3Ta_2O_{15}$	820	H_2O	https://doi.org/10.1016/j.nanoen.2025.110892
9	$Bi_4W_{0.5}Ti_{0.5}O_8Cl$	530.4	H_2O	https://doi.org/10.1016/j.cej.2023.142777
10	BBT-ACN COF	2500	H_2O	https://doi.org/10.1002/adfm.202424035
11	$MoS_2/MnIn_2S_4$	606.7	H_2O	https://doi.org/10.1021/acsaem.4c03296
12	NMP	2552.5	H_2O	https://doi.org/10.1016/j.apcatb.2024.124856
13	$SrCoO_3$-MoS_2	H_2O	H_2O	https://doi.org/10.1016/j.apcatb.2024.124565
14	Na-PHI	3480	H_2O	https://doi.org/10.1016/j.apcatb.2024.124586
15	dual-deficient C_3N_4	1031	H_2O	https://doi.org/10.1016/j.apcatb.2024.124645
16	4Cl-H_2PDI/GQD	2484	H_2O	https://doi.org/10.1016/j.jmst.2024.04.028
17	BiOCl/COF	4088.46	H_2O	https://doi.org/10.1016/j.jcis.2025.137544
18	BiOCl/$ZnIn_2S_4$	9670	H_2O	https://doi.org/10.1039/D4QI02806F